Stabilization of Intrazeolitic Cadmium Telluride Nanoclusters by Ion Exchange

ARTICLE *in* CHEMISTRY OF MATERIALS · AUGUST 1996

Impact Factor: 8.35 · DOI: 10.1021/cm960045s

4 AUTHORS, INCLUDING:

Carl Weisbecker
Sun Chemical
23 PUBLICATIONS **581** CITATIONS
SEE PROFILE

Walter E Rudzinski
Texas State University
77 PUBLICATIONS **3,021** CITATIONS
SEE PROFILE

Stabilization of Intrazeolitic Cadmium Telluride Nanoclusters by Ion Exchange

Elaine S. Brigham,† Carl S. Weisbecker,† Walter E. Rudzinski,‡ and Thomas E. Mallouk*,†

Departments of Chemistry, The Pennsylvania State University, University Park, Pennsylvania 16802, and Southwest Texas State University, San Marcos, Texas 78666

Received January 23, 1996. Revised Manuscript Received April 4, 1996⊗

Cadmium telluride nanoclusters were prepared by vapor-phase deposition of elemental tellurium in Na^+−zeolite A, followed by partial exchange of the zeolite with aqueous $Cd(NO_3)_2$, and reduction with hydrogen at 450 °C. The stability of the nanoclusters in environments that normally cause rapid Ostwald ripening or oxidation (air, water, and Br_2/MeOH) was greatly enhanced by exchanging the Na^+−zeolite with K^+ after the Te^0 deposition and hydrogen reduction steps. Exchange of K^+ for Na^+ narrows the effective pore diameter of zeolite A from 4.0 to 3.3 Å, inhibiting the diffusion of larger atoms, ions, and molecules (Te^0, Te^{2-}, and Br_2). Distinct absorption maxima in diffuse reflectance UV−visible spectra and sharp exciton peaks in low-temperature excitation spectra verified the presence of quantum-confined CdTe. These spectral features are largely unchanged when the material, in its K^+-exchanged form, is exposed to air and water for periods of months. Under the same conditions, materials in the Na^+ form are rapidly degraded. TEM micrographs of the K^+-exchanged materials show 20−50 Å diameter nanoclusters dotted throughout the zeolite matrix. The partial loss of host crystallinity observed in X-ray diffraction patterns suggests that the process of cluster formation involves aggregation within the large cages of the zeolite and local destruction of the pore network.

Semiconductor nanoparticles have been the subject of intensive investigation over the past several years. Apart from their longstanding applications in optical filters and hair-coloring products,[1] these particles have aroused renewed interest because of their interesting physics[2] and the potential of unique applications in solar energy conversion and photocatalysis,[3−5] electronics,[6−10] nonlinear optics,[11−16] electroluminescent displays,[17] and photoluminescent sensors.[18] The progression of electronic and optical properties of these semiconductor particles from bulklike to molecular, as their size is decreased, is now well understood theoretically.[19,20]

The physical and chemical properties of semiconductors change markedly in the nanometer size regime, because the ratio of surface-to-bulk atoms increases with decreasing size. The high surface free energy of these nanoclusters is manifested in unusual crystal structure transformations and particle shapes,[2b] as well as enhanced (surface) reactivity. Control of the surface chemistry is a necessary prerequisite to nanoparticle synthesis and is also important in all of the potential applications mentioned above. Invariably, some clever "capping" chemistry is needed in order to stabilize the surface atoms, lest the particles aggregate or ripen to form bulklike materials.[21] Among the most spectacular recent examples of a capping technique are the crystallization of single-size, capped $Cd_{32}S_{14}(SC_6H_5)_{36}$ clusters and the use of strongly coordinating, high-boiling sol-

† The Pennsylvania State University.
‡ Southwest Texas State University.
⊗ Abstract published in *Advance ACS Abstracts,* July 15, 1996.

(1) The active ingredient in Grecian Formula is a Pb^{2+} salt, which combines with sulfur to produce quantum-size PbS clusters. The progression of colors from yellow to brown to black arises from the steadily increasing particle size, and decreasing optical bandgap, with continued application.

(2) (a) Brus, L. *J. Phys. Chem.* **1986**, *90*, 2555. (b) Alivisatos, A. P. *MRS Bull.* **1995**, *20*(8), 23. (c) Brus, L. E.; Szajowski, P. F.; Wilson, W. L.; Harris, T. D.; Schuppler, S.; Citrin, P. H. *J. Am. Chem. Soc.* **1995**, *117*, 2915.
(3) Kamat, P. V. *Chem. Rev.* **1993**, *93*, 267−300.
(4) Hagfeldt, A.; Grätzel, M. *Chem. Rev.* **1995**, *95*, 49−68.
(5) Weller, H. *Adv. Mater.* **1993**, *5*, 88−95.
(6) Beaumont, S. P. In *Low-Dimensional Structures in Semiconductors*; Peaker, A. R., Grimmeiss, H. G., Eds.; Plenum Press: New York, 1991; pp 109−121.
(7) Schulz-Ekloff, G. In *Zeolite Chemistry and Catalysis*; Jacobs, P. A., Ed.; Elsevier: Amsterdam, 1991; pp 65−78.
(8) Haas, H.; Gentile, P.; Magnea, N.; Pautrat, J. L.; Le Si Dang; Pelekanos, N. T. *Mater. Sci. Eng. B* **1993**, *21*, 224−227.
(9) Abram, I. I. In *Nonlinear Optics in Solids*; Springer-Verlag: Aalborg, Denmark, 1989; pp 190−212.
(10) *MRS Bull.* **1989**, *14*, 12.
(11) Herron, N.; Wang, Y.; Eddy, M. M.; Stucky, G. D.; Cox, D. E.; Moller, K.; Bein, T. *J. Am. Chem. Soc.* **1989**, *111*, 530−540.
(12) Brus, L. *J. Phys. Chem.* **1986**, *90*, 2555.
(13) Cox, S. D.; Gier, T. E.; Stucky, G. D.; Bierlein, J. *J. Am. Chem. Soc.* **1988**, *110*, 2986.
(14) (a) Stucky, G. D. *Prog. Inorg. Chem.* **1992**, *40*, 100−177. (b) Stucky, G. D.; MacDougall, J. E. *Science* **1990**, *247*, 609.
(15) Wang, Y.; Suna, A.; Mahler, W.; Kasowski, R. *J. Chem. Phys.* **1987**, *87*, 7315−7322.
(16) Wang, Y.; Herron, N. *J. Phys. Chem.* **1988**, *92*, 4988−4994.
(17) Colvin, V. L.; Schlamp, M. C.; Alivisatos, A. P. *Nature* **1994**, *370*, 354.
(18) Lauerhaas, J. M.; Credo, G. M.; Heinrich, J. L.; Sailor, M. J. *J. Am. Chem. Soc.* **1992**, *114*, 1911.
(19) Brus, L. E. *J. Chem. Phys.* **1983**, *79*, 5566.
(20) Ramakrishna, M. V.; Friesner, R. A. *J. Chem. Phys.* **1992**, *96*, 873.
(21) Steigerwald, M. L.; Alivisatos, A. P.; Gibson, J. M.; Harris, T. D.; Kortan, R.; Muller, A. J.; Thayer, A. M.; Duncan, T. M.; Douglass, D. C.; Brus, L. E. *J. Am. Chem. Soc.* **1988**, *110*, 3046.

S0897-4756(96)00045-2 CCC: $12.00

vents in the synthesis of crystalline and monodisperse CdSe nanoclusters, which pack in the solid state as opal-like supercrystals.[22]

Microporous solids, such as zeolites and clays, provide a useful matrix for arresting the growth of semiconductor nanoparticles and passivating their surfaces. Various semiconductors, including II−VI compounds, Ge, Si, silver halides, and metal oxides have now been successfully prepared as quantum dots and characterized spectroscopically in zeolite hosts.[11,12,16,23−31] For intrazeolitic II−VI clusters, the simplest and most commonly used synthetic strategy is to ion-exchange the appropriate cation (Cd^{2+}, Zn^{2+}, Pb^{2+}) into the zeolite and then add the anion as a gaseous hydride (H_2S, H_2Se, H_2Te). Apart from the difficulty of handling the latter reagents, this reaction is inconveniently reversible. In a dry environment, extensive pumping liberates H_2X and regenerates the M^{2+}-exchanged zeolite. In wet environments, Ostwald ripening occurs, because of the high surface free energy of the clusters and the ease with which H_2X and M^{2+} can migrate through the zeolite. For example, CdS and CdSe quantum dots prepared in this way are unstable to aggregation upon exposure to air or moisture.[32]

It is widely appreciated that the effective size of the windows connecting zeolite cages changes with the composition of extraframework cations.[33] For example, the 8-ring windows in zeolite A, which connect the large cages in the structure, may have effective diameters of 4.3, 4.0, or 3.3 Å, depending on whether the cation is Ca^{2+}, Na^+, or K^+. In this paper we present a new strategy for preparing stable II−VI nanoclusters in zeolite A. The atomic components of the cluster are loaded into the zeolite in the relatively open Na^+ form, and subsequent ion-exchange with K^+ narrows the pores, preventing corrosion and Ostwald ripening. Control experiments show that these processes are very rapid in the open forms (Na^+ or Ca^{2+} exchanged) of the zeolite.

Experimental Section

Materials. Zeolite 4A was obtained as 2−3 μm size particles from UOP molecular sieves. Elemental analyses gave weight percent values of Al 18.2%, Si 20.0%, Na 12.2%, corresponding to a Si/Al molar ratio of 0.99. The manganese and iron contents of the as-received zeolite were respectively <0.03% and 0.04% by weight. Elemental Te (99.9%) and all other chemicals were obtained from Aldrich and used as received. All aqueous solutions were prepared from 18.3 MΩ cm water, which was obtained from a Barnstead Nanopure system.

Instrumentation. Elemental analyses of samples were run on a Leeman Labs PS3000UV inductively coupled plasma spectrophotometer. Five ICP standards were run prior to each determination. Transmission electron microscopy (TEM) was performed on a JEOL 1200EXII instrument. Sample 1 (see below) was used as prepared and placed on Formvar-coated copper grids. Sample 2 was embedded in a hard-grade resin, and polymerized for 24 h at 50 °C. The sections were microtomed to 70 nm thickness and collected on Formvar-coated copper grids. Powder X-ray diffraction was run on a Philips X'Pert MPD system.

Absorption and Emission Spectroscopy. UV−visible spectral data for powdered samples were collected with a Varian DMS 300 spectrometer fitted with an integrating sphere diffuse reflectance accessory. The spectrophotometer measures reflectance relative to a background scatterer, which was powdered $BaSO_4$. The spectra used for the bandgap calculations are plotted in terms of $F(R)$, the Kubelka−Munk function. The diffuse reflectance, R, of the sample is related to the Kubelka−Munk function by eq 1,[34] where K is the

$$F(R) = (1 - R)^2/2R = K/S \qquad (1)$$

absorption coefficient and S is the scattering coefficient. Emission spectra were collected with a SPEX Fluorolog F212 double-monochromator spectrophotometer, using right-angle detection. The samples were suspended in a solution of EPA (a mixed solvent consisting of 5:5:2 v/v/v diethyl ether: isopentane:ethanol) according to the procedure used by Miyazaki and Yoneyama.[25] A 2 mg sample in 2.5 mL of EPA was placed in a cryogenic cuvette and degassed. A cryostat was used to control the sample temperature between 298 and 77 K.

Preparation of Zeolite-Encapsulated CdTe Nanoclusters. Zeolite 4A was dried for 48 h at 500 °C under flowing argon in a tube furnace. Dry zeolite (4.0 g) was intimately mixed with 0.2 g of Te in an argon-atmosphere drybox and placed in an open-ended tube fitted with a Whitey valve. The tube was sealed under vacuum and then heated to 450 °C in a tube furnace for 3 days. The contents of the sealed tube were transferred in the drybox to a 250 mL Schlenk flask. Degassed aqueous 1 M K_2CO_3 (100 mL) was added to the flask, and the suspension was stirred under argon for 24 h. The suspension was allowed to settle, and the supernatant was removed via cannula. This step was repeated with fresh K_2CO_3 solution. A stoichiometric amount of degassed 0.03 M aqueous $Cd(NO_3)_2$ was then added and stirred for 48 h with the K^+-exchanged Te^0 zeolite A. The supernatant was removed, and the zeolite was transferred in the drybox to an alumina boat, which was placed inside a glass tube fitted with stopcocks. The sample was heated in a tube furnace under flowing hydrogen at 450 °C for 24 h. The cooled sample was then transferred to a 250 mL Schlenk flask, and a stoichiometric amount of K^+−*tert*-butoxide was added. Dry, degassed methanol was added, and the suspension was stirred for 24 h. The supernatant was removed, and the sample was washed three times with 100 mL of methanol. 100 mL of 1% Br_2 in methanol was added to the zeolite and stirred for 24 h. After washing three times with 100 mL aliquots of methanol, the zeolite was dried and then washed several times with water.

(22) (a) Herron, N.; Calabrese, J. C.; Farneth, W. E.; Wang, Y. *Science* **1993**, *259*, 1426. (b) Kagan, C. R.; Murray, C. B.; Bawendi, M. G. *Mater. Res. Soc. Symp. Proc.*, **358** (*Microcrystalline and Nanocrystalline Semiconductors*); Materials Research Society: Pittsburgh, 1995; pp 219−224. (c) Murray, C. B.; Kagan, C. R.; Bawendi, M. G. *Science* **1995**, *270*, 1335.

(23) Wang, Y.; Herron, N. *J. Phys. Chem.* **1987**, *91*, 257−260.

(24) Parise, J. B.; MacDougall, J. E.; Herron, N.; Farlee, R.; Sleight, A. W.; Wang, Y.; Bein, T.; Moller, K.; Moroney, L. M. *Inorg. Chem.* **1988**, *27*, 221−228.

(25) Miyazaki, S.; Yoneyama, H. *Denki Kagaku Oyobi Kogyo Butsuri Kagaku* **1990**, *58*, 37−40.

(26) (a) Ozin, G. A.; Kuperman, A.; Stein, A. *Angew. Chem., Int. Ed. Engl.* **1989**, *28*, 359. (b) Ozin, G. A.; Ozkar, S.; Stucky, G. D. *J. Phys. Chem.* **1990**, *94*, 7562. (c) Stein, A.; Ozin, G. A.; Stucky, G. D. *J. Am. Chem. Soc.* **1990**, *112*, 904. (d) Ozin, G. A. *Adv. Mater.* **1992**, *4*, 612. (e) Ozin, G. A.; Ozkar, S. *Adv. Mater.* **1992**, *4*, 11. (f) Ozin, G. A.; Ozkar, S.; Prokopowicz, R. A. *Acc. Chem. Res.* **1992**, *25*, 553. (g) Ozin, G. A.; Stein, A.; Macdonald, P. M.; Stucky, G. D.; Jelinek, R.; Pines, A. *J. Am. Chem. Soc.* **1992**, *114*, 5171.

(27) Moran, K. L.; Ott, Andrew, W.; Gier, Thurman E.; Harrison, William T. A.; Eckert, Hellmutt; Stucky, Galen D. In *Mater. Res. Soc. Symp. Proc.—Mater, Issues Microcryst. Semiconduct.* **1990**, 123−8.

(28) Herron, N.; Wang, Y. In *Inclusion Phenomena and Molecular Recognition*; Plenum: New York, 1990; pp 401−7.

(29) McMurry, L.; Holmes, A. J.; Kuperman, Alex; Ozin, G. A.; Ozkar, S. *J. Phys. Chem.* **1991**, *95*, 9448−56.

(30) Schulz-Ekloff, G. *Stud. Surf. Sci. Catal.* **1991**, *69*, 65−78.

(31) Wark, M.; Lutz, W.; Schulz-Ekloff, G.; Dyer, A. *Zeolites* **1993**, *13*, 658−62.

(32) (a) Wark, M.; Schulz-Ekloff, G.; Jaeger, N. I.; Lutz, W. In *Synthesis/Characterization and Novel Applications of Molecular Sieve Materials*; Bedard, R. L., Ed.; Mat*er*. Res. Soc. Symp. Proc. v. 233; Materials Research Society: Pittsburgh, 1991; pp 133−138. (b) Herron, N. *J. Inclus. Phenom. Mol. Recog. Chem.* **1995**, *21*, 283−298.

(33) Breck, D. W. *Zeolite Molecular Sieves*; Wiley: New York, 1974.

(34) Kortum, G. *Reflectance Spectroscopy*; Springer-Verlag: New York, 1969.

Table 1. Elemental Analysis of Typical CdTe−K^+−A Sample[a]

sample	Cd%	Te%	K%	Na%	Al%	Si%
UOP−zeolite−Na^+−A	0.00	0.00	0.00	12.2	18.2	19.5
Te^0−Na^+−A	0.00	4.90	0.00	12.6	15.1	
Te^0−K^+−A	0.00	4.15	16.5	1.99	13.7	
Te^0−Cd^{2+}−K^+−A	3.78	3.91	12.7	1.46	13.8	
CdTe−K^+−A	3.29	3.38	13.6	1.40	11.5	

[a] Weight percent ±0.1%.

A control sample of zeolite A was subjected to the same procedure, except that no cadmium or tellurium was added. The amount of cadmium and tellurium in the samples were determined by inductively coupled plasma analysis. Five ICP standards were run prior to each determination. A maximum of 16 wt % elemental Te (1.3×10^{-6} mol/g of Na^+−A, which corresponds to approximately 2 Te/β-cage) could be included in the zeolite. Samples in the range 3−6% CdTe were used in most experiments. The most consistent absorption edge data and emission data were obtained with these samples. Table 1 shows the elemental analysis of a representative zeolite sample during the course of the preparation of CdTe clusters. A 3.29% Cd/3.38% Te weight ratio corresponds to a molar ratio of 1.1:1 (Cd:Te).

Results and Discussion

Zeolite Structure and Synthesis of Intrazeolitic Cadmium Telluride. The zeolite A structure consists of sodalite (or β) cages, each connected by six four-ring prisms into a simple cubic array. This arrangement produces large α-cages of 11.7 Å diameter, which are bounded by eight sodalite cages. Each α-cage is connected to eight others by 8-ring windows. Because of its high Al/Si ratio, zeolite A contains a high density of charge-compensating extraframework cations. The effective diameter of the 8-ring windows depends strongly on the identity of these ions. In the anhydrous Na^+ and K^+ forms, the 8-ring diameters are 4.0 and 3.3 Å, respectively. The Ca^{2+} ion is similar in size to Na^+; however, because only half as many Ca^{2+} ions are needed to compensate the framework charge, the 8-ring diameter in this case is 4.4 Å. The diameters of Cd^{2+}, Te^0, and Te^{2-} are 1.6, 4.2, and 4.4 Å, respectively. Comparing these ionic and atomic sizes to the size of the 8-ring, it is apparent that the diffusion of Te^0 and Te^{2-} will be much slower in K^+−A than it is in Na^+−A or Ca^{2+}−A. These α-cages are connected to the smaller, 6.6 Å diameter β-cages by 2.2 Å diameter 6-ring windows. At room temperature, therefore, the β-cages should not be accessible to larger species such as Te^0 and Te^{2-}; however, at elevated temperatures the migration of these species into the β-cages should be possible.

Te^0 can be introduced from the vapor phase into zeolite A in the Na^+ form but not in the K^+ form. In the latter case, the attempted vapor-phase incorporation of Te results only in the transport of bulk Te metal to the cold end of the sealed tube. Figure 1 shows a typical UV−visible spectrum of a sample loaded with elemental tellurium and then ion-exchanged under anaerobic conditions with K_2CO_3. The absorbance is fairly constant between 230 and 500 nm and then gradually decreases to zero between 550 and 800 nm. The dark brown color of Te^0−K^+−A is similar to that reported by Olson et al. for tellurium-loaded zeolite Na^+−X.[35] Their

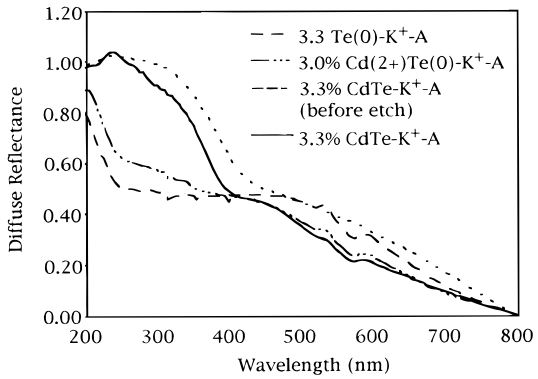

Figure 1. Diffuse reflectance UV−visible spectra of CdTe−K^+−A at various steps in the synthesis: 3.3% Te^0−K^+−A, 3.0% Cd^{2+}−Te^0−K^+−A, and 3.3% CdTe−K^+−A before and after etching with Br_2/methanol.

Te−Na^+−X samples were prepared under conditions identical with those used in the present study for Te^0−A. By way of comparison, zeolites X and A have the same Al/Si ratio and contain the same β-cages. The difference is the manner in which these cages are interconnected. In zeolite X, access to the β-cages is also through 6-ring windows. Olson et al. determined from X-ray diffraction data that Te resides in the β-cages of zeolite X. The similarities in color and the cation dependence of its incorporation into the zeolite suggest that Te^0 is either atomically dispersed in zeolite A, as it is in zeolite X, or present in the α- or β-cages in the form of small clusters. By analogy to the zeolite X case, the most likely site for Te^0 is the β-cages. If one assumes atomic dispersion, at the loadings used in this study (3−6 wt % Te), approximately one- to two-thirds of the β-cages would contain Te atoms.

The loading of zeolite A with Te^0 is followed by exhaustive ion-exchange of the solid with aqueous K_2CO_3. In this process, extraframework Na^+ is replaced by K^+, although a small amount of Na^+ (see Table 1) remains, most probably in the β-cages. Stoichiometric Cd^{2+} is then introduced by ion-exchange with aqueous $Cd(NO_3)_2$. It should be noted that the ionic radius of Cd^{2+} is quite similar to that of Ca^{2+}, and so exhaustive exchange of Cd^{2+} for K^+ results in relatively open zeolite. However, at the low Cd^{2+} loadings used in this study, the predominant extraframework ion is still K^+. The addition of Cd^{2+} produces only small changes in the UV−visible spectrum (Figure 1), which still shows predominantly the features of Te^0−K^+−A.

The reduction of Cd^{2+}−Te^0−K^+−A by H_2 is carried out at the same temperature at which Te^0 is introduced into Na^+−A. This reduction step is followed by a second ion-exchange step under anhydrous, basic conditions (to replace H^+ by K^+), and then by an etch with Br_2/methanol to remove any CdTe or Te^0 from the external surface of the zeolite. The synthetic procedure is outlined in Scheme 1, and UV−visible spectra corresponding to the synthesis steps are shown in Figure 1. One expects that, if Te^0 is indeed located in the β-cages, it should be able to migrate back through the six-ring windows connecting the α- and β-cages at the reduction temperature, and that Cd^{2+} should also migrate freely between cages. The reaction of these species to produce intrazeolitic CdTe is strongly suggested by a prominent absorption band that appears in the UV part of the

(35) Olson, D. H.; Mikovsky, R. J.; Shipman, G. F.; Dempsey, E. *J. Catal.* **1972**, *24*, 161−169.

Scheme 1. Synthesis of Intrazeolitic $(CdTe)_n$ Clusters

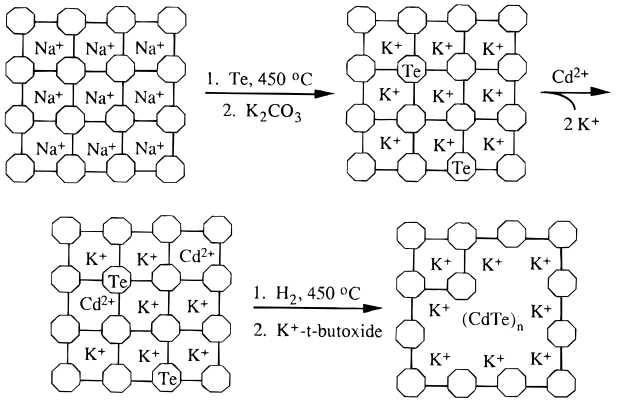

spectrum. The fact that most of the semiconductor particles are confined to the interior of the zeolite is confirmed by elemental analysis following the Br_2/methanol etch (Table 1). This etch predominantly attenuates the red tail of the absorption spectrum, suggesting that it dissolves larger, extrazeolitic particles.

Transmission electron micrographs (Figure 2) confirm the synthesis of intrazeolitic nanoclusters. They show a range of particle sizes, between 16 and 51 Å, with a mean value of 30 Å and a standard deviation of 8 Å. Two samples were examined, with essentially the same results. For sample 1, CdTe-loaded zeolite powder was sprinkled onto a TEM grid, and images were obtained from the small fraction of particles that were thin enough to transmit the electron beam. In sample 2, the CdTe-loaded zeolite was embedded in a hard resin and microtomed, and therefore these images should be more representative of the bulk material. In neither case does a significant fraction of the CdTe appear to have migrated to the external surface of the zeolite.

X-ray Powder Diffraction. Figure 3 compares powder diffraction patterns of hydrated, K^+-exchanged zeolite A to samples obtained after each of the synthesis steps leading to the formation of CdTe clusters. In all cases, only peaks attributable to the zeolite host are observed. As the relative intensities of the peaks do not change significantly, it can be concluded that none of the heavy atoms order within the zeolite framework. A very slight contraction is seen in the lattice parameter of the zeolite, consistent with small changes in extraframework composition during the progression of synthesis steps. A significant decrease in peak intensities, which occurs during the last step, signals some loss of framework crystallinity upon reduction of Cd^{2+}–Te^0 to CdTe. These observations are consistent with the TEM images, which show particles dotted randomly through the zeolite.

It is interesting to note that the average cluster size inferred from TEM (and from electronic spectra, see below) is 2–3 times the size of the α-cage. These results are reminiscent of those of Miyazaki and Yoneyama, who prepared CdS and CdSe clusters in zeolite A. They found that the diameter of the crystallites was about twice the diameter of the α-cage (11.7 Å).[25] They attributed this behavior to the aggregation of semiconductor particles along the channels of the zeolite. It is possible that "superclusters" [11] consisting of neighboring filled α-cages are formed in the present case as well,

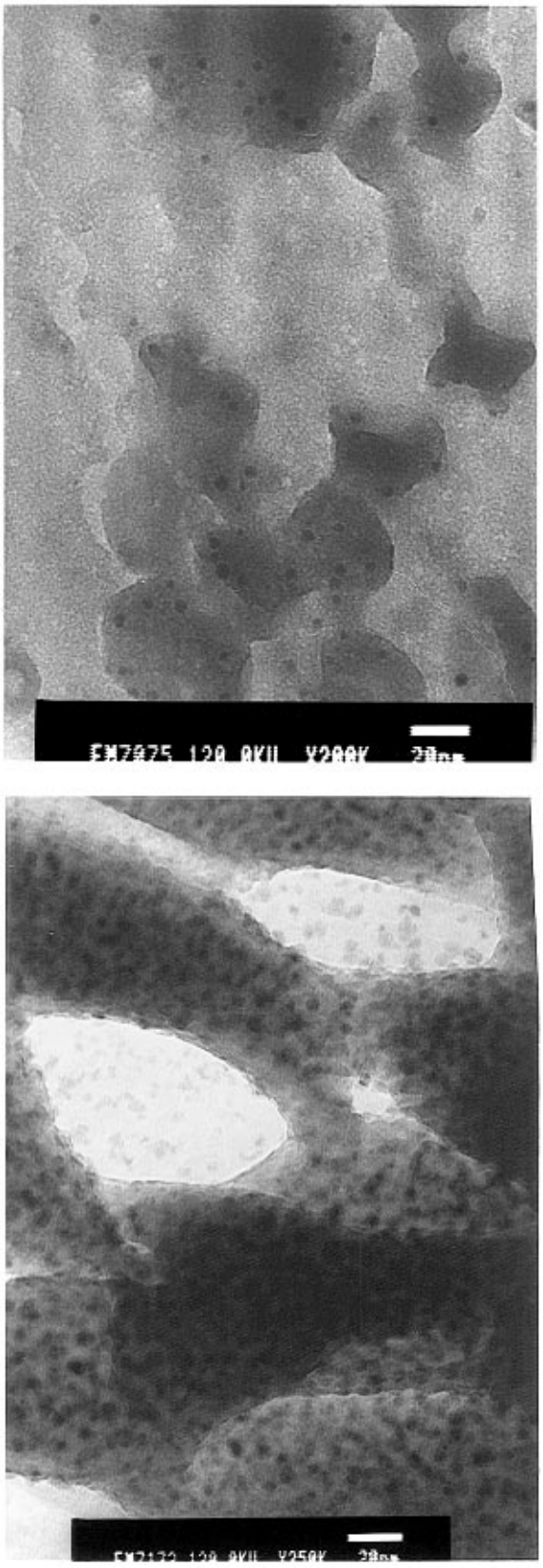

Figure 2. Transmission electron micrographs of 3.3% CdTe–K^+–A (a, top) as prepared and (b, bottom) embedded in a hard resin and microtomed into thin sections. Scale bar is 20 nm.

and their internal structure is not resolved in TEM. An alternate explanation, which is supported by the loss of zeolite diffraction intensity, is that the framework is disrupted in the vicinity of the clusters, allowing them to grow larger than the size of the α-cage. In either case it is clear that both Cd^{2+} and Te^0 must have sufficient

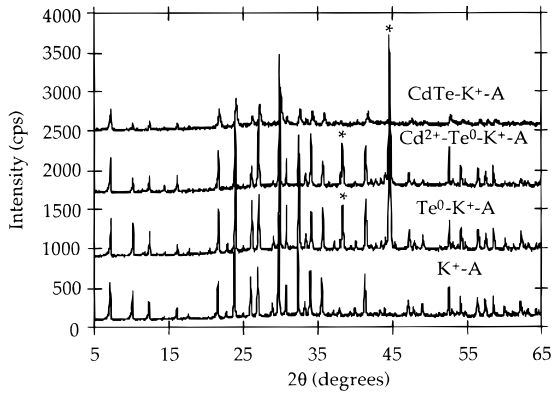

Figure 3. X-ray powder diffraction patterns of K^+-A, Te^0-K^+-A, $Cd^{2+}-Te^0-K^+-A$, and $CdTe-K^+-A$ (4%). Asterisks denote lines from the aluminum sample holder. The cubic lattice parameters are 24.70 (2), 24.58 (2), 24.61 (2), and 24.49 (3) Å, respectively.

mobility at the reduction temperature to form aggregates containing at least a few hundred atoms. The mobility of Te^0 or of CdTe, once formed, is apparently not sufficient to drive the system to its lowest free energy state, i.e., to form bulk CdTe crystallites on the external surface of the particles. The lack of mobility on this larger length scale is of course consistent with the observation that Te^0 cannot be introduced into K^+-A to any significant extent at an even higher temperature.

Electronic Spectra and Quantum Size Effects. The spectrum of $CdTe-K^+-A$ (Figure 1) shows a structured ultraviolet absorption, with a maximum at 230 nm and shoulder at 320 nm, that is reminiscent of previously reported quantum-confined 12−16 semiconductor particles.[11,13−17,23−25] The visible absorption feature that tails to the red is similar to that of the Te^0-K^+-A sample and is tentatively attributed to residual Te^0 in the zeolite.

The ultraviolet absorption onset that appears at 380−400 nm can be attributed to a bandgap transition. The bandgaps of the CdTe-loaded zeolites were calculated from their diffuse-reflectance spectra by plotting the square of the Kubelka−Munk function, $F(R)^2$ vs energy in electronvolts. For a direct bandgap semiconductor, such as CdTe,[36] one expects a linear relationship between the square of the absorbance and the excitation energy above the bandgap energy. Extrapolating this linear region of the transformed spectrum (Figure 4) to zero, we obtain an optical bandgap of 3.35 eV (370 nm) for a 4% $CdTe-K^+-A$ sample. From the optical bandgap, one can estimate the average particle size using eq 2,[15,37] in which E_g' is the quantum-confined bandgap,

$$E_g' = [E_g^2 + (2\hbar^2/m^*)(\pi/R)^2 E_g]^{1/2} \qquad (2)$$

E_g is the bulk bandgap for the semiconductor, m^* is the reduced mass ($1/m^* = 1/m_e + 1/m_h$), m_e and m_h are, respectively, the electron and hole effective masses, and R is the radius of the nanocluster. From this equation, using values of 0.14 and 0.35 for m_e and m_h,[25] respectively, a particle diameter of approximately 20 Å is obtained. Average particle diameters between 19 and 29 Å were calculated in this way for various samples, with no obvious correlation between the loading of CdTe and the optical bandgap. These particle diameters are completely consistent with the TEM images shown in Figure 2.

(36) Zanio, K. *Cadmium Telluride*; Academic Press: New York, 1978; Vol. 13, p 84.
(37) Brus, L. E. *J. Chem. Phys.* **1984**, *80*, 4403−4409.

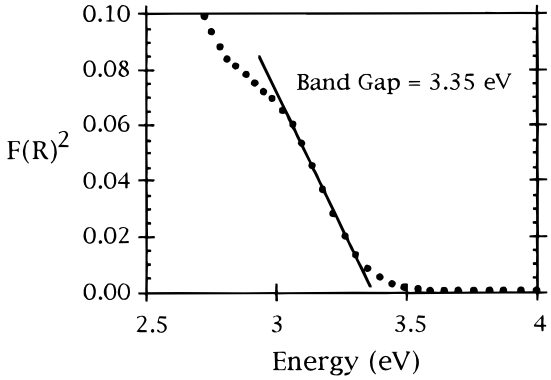

Figure 4. Plot of $F(R)^2$ vs energy of reflected light for 4% $CdTe-K^+-A$. The line through the data is extrapolated to $F(R)^2 = 0$ to give the optical bandgap.

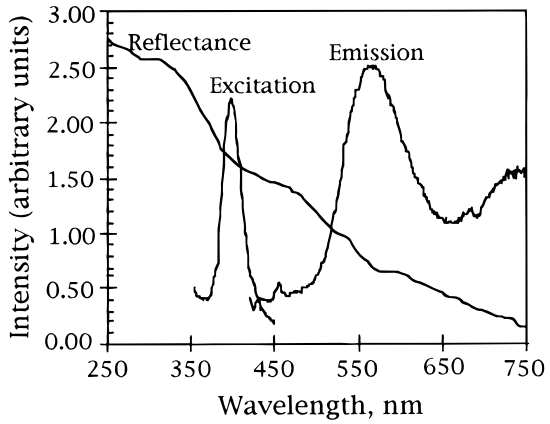

Figure 5. Room-temperature diffuse reflectance and 77 K excitation and emission spectra of 4% $CdTe-K^+-A$.

Emission Spectroscopy. Figure 5 shows the excitation and the emission spectra of a 4% CdTe−K−A zeolite sample at 77 K. The excitation spectrum shows a pronounced peak at 390−400 nm, very near the edge of the CdTe absorption spectrum. The long-wavelength tail of the absorption spectrum may be attributed to residual Te^0, which is present to varying degrees in all the samples studied. Wang and Herron attributed the sharp excitation peaks at 320−360 nm of CdS clusters in zeolites A, X, and Y to an exciton transition.[16] The position of the sharp excitation peak in Figure 5 also strongly suggests that it is excitonic.

The emission spectrum at 77 K shows a broad peaks centered at 563 and 750 nm. There is no emission at shorter wavelengths, near the optical bandgap, and therefore direct electron−hole recombination does not contribute significantly to the emission spectrum. The emission peaks therefore arise from defects. Figure 6 shows the emission spectrum as a function of temperature. Wang and Herron[16] have analyzed in some detail the temperature-dependent emission spectrum of CdS in zeolite A, which has peaks at 440, 580, and 660 nm. They attributed the 560−580 emission to the transition from midgap states localized on Cd atoms to the valence band of quantum-confined CdS. The red emission was attributed to midgap states associated with sulfur

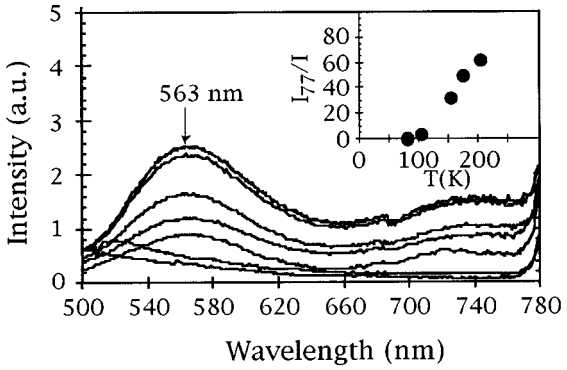

Figure 6. Variable-temperature emission spectra of 4% CdTe−K^+−A. Temperatures (top to bottom) are 77, 100, 150, 170, 200, 250, and 298 K. The inset shows the variation of the 563 nm peak intensity, plotted as I_{77}/I_T, between 77 and 200 K.

vacancies. Because the absorption spectra show evidence for residual Te^0 in our samples, it follows from the overall 1:1 stoichiometry that the $(CdTe)_n$ clusters in K^+−A are cadmium-rich. A plausible model for these clusters, considering the anionic nature of the zeolite host, is that they are capped by Cd^{2+} ions. It is therefore not unreasonable to expect trap emission from excess Cd and from Te vacancies, to which we tentatively assign the 563 and 750 nm emission bands.

The temperature dependence of the 563 nm CdTe−K^+−A reciprocal emission intensity, shown in the inset of Figure 6, is slight between 77 and 100 K and then more pronounced between 100 and 200 K. This non-Arrhenius temperature dependence is characteristic of a relaxation process dominated by multiphonon-induced radiationless decay.[38] Wang and Herron[16] determined that in the case of CdS in zeolite A the interface (Cd−O) and zeolite host (Si−O and Al−O) phonons with average frequencies in the range 500−600 cm^{-1} mediate the radiationless relaxation process. They estimated the highest frequency of intracluster (Cd−S) vibrations to be below 300 cm^{-1}, which is too low to contribute substantially to nonradiative decay. These intracluster phonons will have even lower frequencies in the case of CdTe. Because we observe a very similar temperature dependence, the same relaxation mechanism is likely to be operative in the present case.

Variation of the 8-Ring Window Size by Cation Exchange. Experiments were done to determine the effect of the window size on the stability of CdTe nanoclusters in zeolite A. The samples were prepared as discussed in the experimental section except for these adjustments: After Te^0 was vapor deposited into the zeolite, the window size was adjusted by exchange with either Na^+, K^+, or Ca^{2+} ions in the form of their carbonate salts. All subsequent steps were the same except for the deacidification step. For the sodium zeolite, sodium methoxide was the base employed, and calcium ethoxide was used for the calcium zeolite. Figure 7 shows the effect of the Br_2/methanol etch on the spectrum of the semiconductor clusters. In the sodium exchanged sample, an absorption edge appears at about 330 nm but disappears upon etching with Br_2/methanol. The contrast with the behavior of CdTe−K^+−A (Figure 1) is quite dramatic. The kinetic diameter of Br_2 is 3.5 Å.[33] This is too large to penetrate rapidly into the zeolite in the K^+ form but is sufficiently small to completely react with CdTe encapsulated by (4.3 Å) Na^+−A. In this case, there is some residual absorbance from Te^0, which is probably located in the β-cages and therefore inaccessible to Br_2.

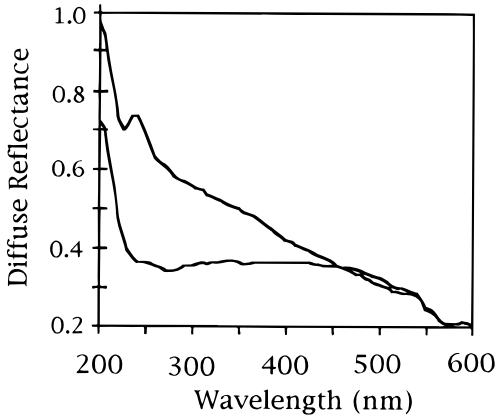

Figure 7. Effect of Br_2/methanol etching on the UV−visible spectrum of 5% CdTe−Na^+−A. Spectral features attributed to CdTe (upper trace) are lost upon etching (lower trace). Residual visible absorbance is attributed to Te^0.

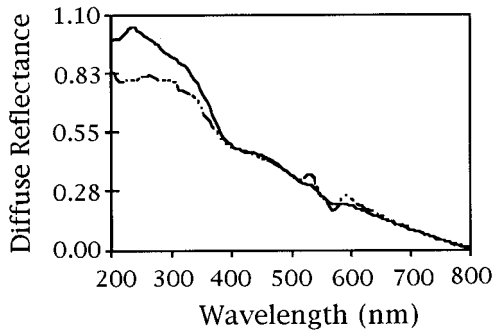

Figure 8. UV−visible spectrum of 3.3% CdTe−K^+−A upon preparation (upper trace) and after aging in air for 6 months.

Figure 8 shows the diffuse reflectance spectrum of a 3.3% CdTe−K^+−A sample after 6 months exposure to the ambient atmosphere. A change in the maximum absorbance is observed, but the absorption edge is not greatly affected. Exposure of these samples to Br_2/methanol has little effect on these spectral features. Although water molecules can easily pass through the 3.3 Å windows, Ostwald ripening is curtailed by the K^+ ions, because Te^0 and Te^{2-} are too large to exit. Likewise, Br_2 is too large to enter, and so there is minimal oxidation of the clusters. By way of comparison, Wang and Herron observed a rapid shift of the absorption edge toward the red when they exposed mordenite-confined CdS nanoclusters to atmospheric moisture.[23] The CdTe clusters reported in this study are inherently more stable than II−VI clusters prepared in the sodium and calcium forms of zeolite A, or II−VI clusters grown in larger-pore zeolites.

Conclusions

A new strategy for preparing stable semiconductor nanoclusters in zeolite A has been presented. This method uses an ion exchange reaction to "close the door" to migration of large atoms, ions, and molecules between

(38) (a) Chestnoy, N.; Harris, T. D.; Hull, R.; Brus, L. E. *J. Phys. Chem.* **1986**, *90*, 3393. (b) Fong, F. K. *Theory of Molecular Relaxation. Applications in Chemistry and Biology*; Wiley: New York, 1975.

cages. The components of the semiconductor (Cd^{2+} and Te^0) are loaded into the zeolite in the "open" Na^+ form and are then reduced to form CdTe clusters in the "closed" K^+ form. These clusters show the typical absorption and emission spectral features of intrazeolitic, quantum-confined semiconductor particles. X-ray diffraction patterns suggest local destruction of the zeolite framework where the clusters are formed. The CdTe particles produced by this method appear to be air- and water-stable for 6 months or more. In contrast, similar clusters grown in the open forms of the same zeolite undergo rapid Ostwald ripening and are readily etched by Br_2. This dramatic difference in stability may be understood in terms of the effective size of the windows that interconnect large cages in the zeolite A structure.

Acknowledgment. This work was supported by the Division of Chemical Sciences, Office of Basic Energy Sciences, Department of Energy, under Contract DE-FG02-93ER14374. C.S.W. gratefully acknowledges support from the NSF Summer Program in Solid State Chemistry. Instrumentation for X-ray diffraction experiments was provided by NSF Grant DMR-9402860.

CM960045S